Environmental Pollution 397 (2026) 127940

Contents lists available at ScienceDirect

Environmental Pollution

journal homepage: www.elsevier.com/locate/envpol

Assessment of aerosol optical depth using MAIAC and AERONET data during the 2020 wildfire season in southeastern South America

María Fernanda Valle Seijo [a,b,*], Lidia Ana Otero [c], Alejandro Agesta [d], Erna Frins [d], Rubén Darío Piacentini [a,e]

[a] Instituto de Física Rosario (CONICET - UNR), Blvd. 27 de Febrero 210 Bis, S2000, Rosario, Argentina
[b] Facultad de Química e Ingeniería del Rosario, Pontificia Universidad Católica Argentina (UCA), Av. Pellegrini 3314, S2002QEO, Rosario, Argentina
[c] Facultad de Ingeniería del Ejército, Universidad de la Defensa Nacional, Av. Cabildo 15, C1426AAA, CABA, Argentina
[d] Instituto de Física, Facultad de Ingeniería, Universidad de la República, Av. Julio Herrera y Reissig 565, 11300, Montevideo, Uruguay
[e] Instituto Tecnológico de Diseño e Innovación, Facultad de Ciencias Exactas, Ingeniería y Agrimensura, Universidad Nacional de Rosario, Av. Pellegrini 250, S2000, Rosario, Argentina

ARTICLE INFO

Keywords:
Air quality
Biomass burning
Aerosol properties
Remote sensing

ABSTRACT

Wildfires are major contributors to air pollution, with significant impacts on regional air quality and public health. The objective of this study is to assess aerosol optical depth (AOD) during the intense 2020 wildfire season in southeastern South America. AOD data were retrieved from the MAIAC/MODIS algorithm and fire data from VIIRS/SUOMI-NPP satellite. The satellite AOD was correlated with AERONET measurements over Buenos Aires and Montevideo to evaluate satellite performance during fire periods, with higher correlations expected under smoke dominated conditions. Results for the whole area reveal significantly higher AOD values in 2020, with a median of approximately 0.118. Seasonal analysis highlights notable peaks in fire pixel counts during austral spring (median AOD = 0.154) and winter 2020 (median AOD = 0.114). AERONET observations indicated robust correlations with MAIAC AOD during 2020 (R = 0.75). Moderately strong correlations are observed during winter and spring due to elevated aerosol loads from biomass burning. Specifically, Buenos Aires exhibited changes in the AOD-Ångström Exponent relationship, indicating fine-mode aerosol dominance, while Montevideo displayed less pronounced variability but consistent seasonal patterns. These findings show the impact of biomass burning events on air quality, and the utility of integrating satellite and ground-based data for aerosol analysis.

1. Introduction

Air pollution is responsible for approximately 5.2 million deaths annually (Huang et al., 2024). Particulate matter (PM) refers to solid or liquid particles suspended in the air, typically characterized by their aerodynamic diameter and mass concentration, and it ranks as the leading global risk factor for disease (Brauer et al., 2024). Hence, in 2021, the World Health Organization (WHO) published updated guidelines for annual mean outdoor concentrations of fine particulate matter ($PM_{2.5}$; particles with an aerodynamic diameter equal to or less than 2.5 μm), reducing the previous recommended limit by 50%, from 10 to 5 $\mu g/m^3$, to better protect public health (World Health Organization, 2021).

Wildfires are significant sources of $PM_{2.5}$ due to the vast amounts of particles released during the combustion process (Roberts & Wooster, 2021). Numerous studies have investigated the consequences of wildfires, highlighting their significant impact on human health (Gao et al., 2023; Lei et al., 2024; Rongbin et al., 2020). In South America, recent research has highlighted the growing influence of wildfires on regional air quality over the past decade (Bolaño-Diaz et al., 2022; Cobelo et al., 2023; Guerrero et al., 2024; Krecl et al., 2025; Mollinedo et al., 2023). Furthermore, a study simulating fire conditions in the Amazon region up to 2050 reported that under current scenarios, deforestation could increase the number of fires by 19%, while climate change alone could be responsible for a 12% increase (Silvestrini et al., 2011). Recent works further support the conclusion that projected climate change will substantially heighten the risk of fires in the Amazon (Reis et al., 2021; Mansoor et al., 2022). The Pantanal is the world's largest wetland and

* Corresponding author.
E-mail address: valleseijo@ifir-conicet.gov.ar (M.F. Valle Seijo).

https://doi.org/10.1016/j.envpol.2026.127940
Received 2 July 2025; Received in revised form 17 February 2026; Accepted 7 March 2026
Available online 10 March 2026

extends across Brazil, including the state of Mato Grosso do Sul. This region is commonly affected by fires; however, in 2020, nearly half of the Pantanal burned. Moreover, the area burned in 2020 was 376% higher than the average for 2003–2019 (Garcia et al., 2021).

Over the last years, satellite remote sensing of particulate pollution has advanced significantly, particularly with the launch of NASA's Terra and Aqua missions, which have provided unprecedented datasets for monitoring atmospheric aerosols (Remer et al., 2024; Si et al., 2021). Aerosol Optical Depth (AOD), a dimensionless metric that represents the optical thickness or column-integrated aerosol loading in the atmosphere, has been used to estimate $PM_{2.5}$ (Christopher & Gupta, 2020; Fathollahi et al., 2023; Li et al., 2021). The Multi-Angle Implementation of Atmospheric Correction (MAIAC) algorithm (Lyapustin et al., 2018) has been extensively used in studies to retrieve AOD, offering a spatial resolution of approximately 1 km × 1 km and a daily temporal resolution (Mhawish et al., 2019; Zhang et al., 2019). The MAIAC AOD data are obtained from the Moderate Resolution Imaging Spectroradiometer (MODIS) onboard Terra and Aqua, and has been validated on a global scale (Qin et al., 2021) and in regional studies (Ștefănie et al., 2023; Abuelgasim et al., 2021).

While satellite-derived AOD provides valuable large scale coverage, it is often complemented by ground-based observations. Previous studies have shown that hybrid approaches that combine satellite observations with in situ monitoring offer a more accurate assessment of air quality (Apte & Manchanda, 2024; Kaufman et al., 2002). The AERONET (Aerosol Robotic Network) serves as a globally distributed network of ground-based sun photometers and sky radiometers specifically designed to measure and monitor spectral AOD and other derived atmospheric aerosol properties (Holben et al., 1998, 2001). Managed by NASA in collaboration with global partners, AERONET provides consistent, high-quality data essential for understanding aerosol types and their impacts on climate, air quality, and atmospheric processes (Lee et al., 2010; Mielonen et al., 2009). In South America, Martins et al. (2017) validated satellite-derived AOD from MAIAC using AERONET stations; however, their analysis only extended through 2016 and did not include the Montevideo station, which began operation in 2020.

Previous studies have shown that downscaling global emission inventories to regional scales can result in large discrepancies in the identification of pollution sources. This reinforces the need for regional studies that accurately assess source contributions, especially given the climatic, demographic, and economic heterogeneity across South America (Huneuss et al., 2020). During 2020, fire counts in southeastern South America increased by 113% compared with the 2013–2022 mean (Valle Seijo et al., 2024a) yet the associated aerosol impacts remain poorly quantified. In contrast, Brazil has a substantially larger number of studies evaluating aerosol load, biomass burning, and air-quality impact (Souto-Oliveira et al., 2023). This study therefore aims to: (i) characterize the annual and seasonal patterns of AOD during the 2020 wildfire season using MAIAC satellite observations; (ii) correlate the satellite-derived AOD with ground-based AERONET measurements from Montevideo and Buenos Aires; (iii) assess the influence of wildfires on atmospheric aerosol loading over these cities. The first-time inclusion of the AERONET in Montevideo to validate the MAIAC observations increases the accuracy of the regional aerosol analysis targeted in this work.

2. Materials and methods

2.1. Study area

The study focuses on a region of southern South America that includes parts of Argentina, Uruguay, Paraguay, and southeastern Brazil. Fig. 1 depicts the broader South American context, with a red box that highlights the study area (36.04° S, 21.72° S; 63.39° W, −52.97° W). A zoomed view of the red box shows country borders and details the locations of the AERONET sites in Buenos Aires (CEILAP-BA) and Montevideo (red dots), which provide the ground-based data used in this study.

This region was selected based on its climatic homogeneity and its documented exposure to biomass burning events. According to the Köppen–Geiger climate classification (Peel et al., 2007), the entire area falls under the Cfa category (temperate climate characterized by hot summers and no distinct dry season), indicating that climate variables are relatively uniform across the region and therefore unlikely to

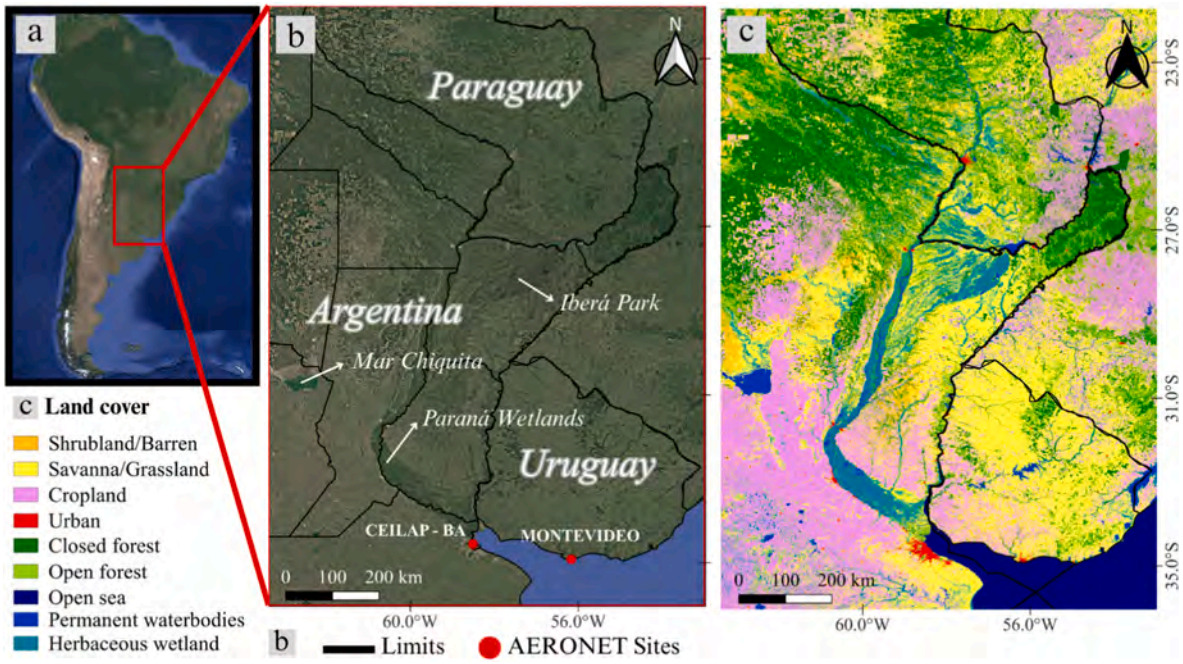

Fig. 1. Maps of the study area and key contextual information. **(a)** Location of the study area in South America (Map source: Google Maps). **(b)** Zoomed-in view of the selected area, showing the positions of AERONET monitoring sites in Buenos Aires (CEILAP-BA) and Montevideo. **(c)** Land cover classification (Source: Copernicus Global Land Service).

account for local particularities. Instead, fire events in this region are primarily driven by land cover characteristics (Fig. 1 c) and local agricultural practices (San Martín et al., 2023). These events are further exacerbated during La Niña episodes, which occur in cycles averaging approximately four years and typically bring prolonged drier conditions to the area. Valle Seijo et al. (2024b) reported that fire events under La Niña (2020-2022) were predominantly concentrated in the northern part of the study region, particularly during winter and spring.

The three land cover types with the highest percentages in the region are savanna/grassland vegetation (30.8%), forest (28.5%), and cropland (23.3%). Urban areas account for only 0.5% of the total area and are primarily concentrated in the capital cities of Argentina (Buenos Aires), Uruguay (Montevideo), and Paraguay (Asunción). These classifications are essential for understanding land use and natural vegetation cover, which are related not only to fire events but also to satellite observation of atmospheric variables, further analyzed in Section 3.

Land cover data were obtained from the CGLS-LC100 product from Copernicus Global Land Service (CGLS). The version 3.0.1 of these maps has a global spatial coverage, and a temporal coverage that goes from 2015 to 2019, derived from the PROBA-V 100 m time-series. They are based on a high-quality land cover training sites database and several additional datasets, achieving an accuracy of 80% at Level 1 across all years (Buchhorn et al., 2020).

2.2. Satellite-Based Aerosol optical depth (MAIAC/MODIS)

The MCD19A2 (V 6.1) is the short name for the MAIAC algorithm-based Level 2 gridded (L2G) aerosol optical thickness over land surfaces product. The product provides satellite-derived AOD in the blue band (470 nm) and green band (550 nm), obtained from MODIS onboard both the Terra and Aqua satellites. This study employs MAIAC AOD at 470 nm, as recommended in the MAIAC algorithm user guide, which reports better validation performance at 0.47 μm than at 0.55 μm. The values are available with a daily temporal resolution and a spatial resolution of 1 km per pixel. This product offers temporal coverage from February 24, 2000, to the present, with global spatial coverage. The MCD19A2 product is accessible through NASA's data distribution platforms. A detailed description of the algorithm, including its capabilities, constraints and latest improvements has been available since its initial publication (Lyapustin et al., 2011, 2012; 2018).

The MAIAC algorithm employs a physical atmosphere–surface model. It begins by gridding MODIS L1B measurements onto a fixed 1 km grid and accumulating data over a time series of up to 16 days using a sliding window approach. This method incorporates numerous independent observations over the same grid cell over time, enabling the separation of atmospheric and surface contributions through time series analysis (Lyapustin et al., 2018). However, this generalized parameterization makes MAIAC retrievals sensitive to shortcomings in surface reflectance modeling, highlighting the importance of studying its implications for accurate assessment.

AOD at 470 nm was analyzed for the area described in Fig. 1. The annual analysis used all daily observations (365 days per year, or 366 in leap years) from January 2018 to December 2022. For the seasonal analysis, data from December 2017 to November 2022 were grouped into the following categories: summer (December–February), autumn (March–May), winter (June–August), and spring (September–November). The satellite-derived AOD values reported in this work were filtered using the Quality Assurance (QA) dataset, specifically applying QA Bits 8–11 set to "0000″ to ensure "Best Quality" data. Maps are included to assess the spatial and temporal distribution of AOD over the region of study. Correlations between satellite-derived AOD and ground measurements from the same variable are also discussed in sections 3.3 and 3.4.

2.3. Satellite-based fire information (VIIRS/S-NPP)

The aerosol data were compared with two fire-related variables: the number of fire pixels and the Fire Radiative Power (FRP). FRP, expressed in megawatts (MW), represents the rate at which energy is radiated by active fires and serves as an indicator of fire intensity. Fire data were obtained from the daily VNP14IMG product, which is derived from the VIIRS 375 m active fire product onboard the Suomi National Polar-orbiting Partnership (S-NPP) satellite. The high spatial resolution (375 m) of the VNP14IMG product enhances the detection of smaller fire areas, thereby improving the accuracy of fire characterization (Schroeder et al., 2014). For this work, daily data underwent filtering based on the confidence attribute. Only data with nominal and high confidence levels were used. For consistency, fire data were grouped using the same annual and seasonal definitions applied to the aerosol dataset.

2.4. AERONET stations

This study uses a global network of ground-based sun photometers (AERONET) developed and managed by NASA in collaboration with institutions worldwide. It provides high-quality AOD data, every 15 min interval for over 30 years in some regions. Based on Beer Lambert-Bouguer law, it computes columnar AOD from 340 to 1020 nm with expected uncertainty of approximately 0.01 to 0.02 (Eck et al., 1999). This data has been widely used for validating satellite-derived AOD globally (Chu et al., 2002; Ichoku et al., 2002; Sayer et al., 2013) including in South America, where this study's focus region is located (Martins et al., 2017). The Buenos Aires AERONET site (Fig. 1c) is equipped with a CIMEL solar photometer that provides daylight observations. By contrast, the CE318-T photometer deployed in Montevideo enables both daytime and nighttime measurements, with retrievals available at 3-min intervals (Barreto et al., 2016).

2.4.1. Ground-Based Aerosol optical depth

This study utilized Level 2 AOD Version 3 data, which includes pre and post-field calibration, cloud-screening, and quality assurance for high reliability. Advancements in the AERONET Version 3 database, as outlined by Giles et al. (2019), further enhance the accuracy and robustness of this dataset.

AOD at 440 nm data was collected from two AERONET sites: CEILAP-BA station (34.55° S, 58.50° W) and Montevideo_FING station (34.9° S, 56.16° W). The CEILAP-BA station provided continuous data coverage for the entire study period (2018-2022), while Montevideo station, a newer addition to the AERONET network, has data available from 2020 to 2022. Two other AERONET stations in our study region were excluded due to limited temporal coverage and data quality below Level 2, which hindered statistical evaluation. Given the extent of the study area, this represents a limitation. Additional ground-based measurements are needed to fully assess performance across the entire region. Therefore, the AERONET results should be considered valid only for the Montevideo and Buenos Aires metropolitan areas.

Martins et al. (2017) evaluated multiple combinations of spatial and temporal windows to optimize comparisons of AOD data from MAIAC (MODIS – Terra/Aqua) with AERONET stations. Based on their findings, this study adopted a spatial window of 25 × 25 km^2 and a temporal window of ±60 min. For the spatial window, we calculated the mean MAIAC-MODIS AOD values (from both Aqua and Terra) at 470 nm over a 25 × 25 km^2 area centered on the pixels corresponding to each AERONET station. For the temporal window, we calculated the mean AERONET AOD at 440 nm recorded within ±60 min of the MODIS overpass, distinguishing between Terra and Aqua observations.

For the correlation analysis, scatter plots were generated. The reported statistics include the number of data points (N) and the Pearson correlation coefficient (R). The percentage of points within the expected error (EE) was calculated using Equation (1):

$$EE = \pm (0.05 + 0.05 \times AOD) \quad (1)$$

Moreover, the root mean square error (RMSE) and bias were computed following Equations (2) and (3):

$$RMSE = \sqrt{\left(\frac{1}{n}\sum_{i=1}^{n}(AOD_{MAIAC} - AOD_{AERONET})^2\right)} \quad (2)$$

$$Bias = \frac{1}{n}\sum_{i=1}^{n} AOD_{MAIAC} - AOD_{AERONET} \quad (3)$$

The reported bias between MAIAC (470 nm) and AERONET (440 nm) AOD reflects potential discrepancies due to the small wavelength difference. This bias may partially capture the natural variation in AOD with wavelength, along with algorithmic or instrumental differences between the datasets.

To compare R between groups, we applied Fisher's *z*-transformation (Fisher, 1915). This transformation normalizes the sampling distribution of correlation coefficients, allowing for valid significance testing. Each R was0 transformed using:

$$z = \frac{1}{2}\ln\left(\frac{1+R}{1-R}\right) \quad (4)$$

The standard error for the difference between two transformed correlations was computed as:

$$SE = \sqrt{\frac{1}{N_1 - 3} + \frac{1}{N_2 - 3}} \quad (5)$$

The resulting *z*-values were then compared to assess whether the correlations differed significantly between groups, with statistical significance evaluated at the conventional $\alpha = 0.05$.

2.4.2. Ground-based Ångström Exponent

The Ångström Exponent (AE) is a parameter that characterizes the wavelength dependence of AOD, providing information on aerosol particle size distribution. In this study, AE at 440–670 nm was also obtained from the ground-based sun photometers at the AERONET stations in Buenos Aires and Montevideo. These measurements provided a reliable ground-based indicator for evaluating aerosol properties, particularly during biomass-burning events. A previous study analyzed AE during the 2020 burning season in Brazil using data from a sun photometer and found strong correlations with other aerosol properties, including single-scattering albedo (Vieira et al., 2023). Biomass burning aerosols are typically characterized by AE values between 1 and 2 (Martins et al., 2017).

3. Results and discussion

3.1. Annual variability of MAIAC/MODIS AOD

Interannual patterns in aerosol loading were evaluated using MAIAC/MODIS together with VIIRS/NPP fire data. Table 1 provides an annual summary of AOD values at 470 nm, the number of fire pixels, FRP for southeastern South America from 2018 to 2022. The AOD data, derived from MAIAC/MODIS, includes the 25th percentile (Q1), median (Mdn), and 75th percentile (Q3) values. The number of fire pixels and FRP values (in megawatts) are derived from VIIRS/NPP. The results illustrate interannual variability in aerosol loading and fire activity across the region, with 2020 emerging as a particularly extreme year.

Annual medians were estimated from daily regional medians, and uncertainty was quantified via bootstrap resampling to account for temporal variability. The highest annual median AOD was observed in 2020 (Mdn = 0.118 [0.112–0.126]), together with elevated first and third quartiles (Q1 = 0.087 [0.083–0.097]; Q3 = 0.169 [0.158–0.193]), indicating increased aerosol loading during that year. Comparison with a baseline period, defined using daily median values from 2018, 2019, 2021, and 2022, showed that the 2020 median AOD was significantly higher. The estimated difference between 2020 and the baseline was Δ = 0.011 [0.006–0.019] indicating a statistically significant increase in AOD.

It is important to note that these medians represent values averaged over the entire year and therefore may mask pronounced seasonal or regional peaks further analyzed in section 3.2. In the supplementary material, Fig. S1 shows density maps of the yearly spatial distribution of fire pixels. Fire activity, estimated from the number of fire pixels, also increased in 2020. In that year, 546,893 pixels were detected in the analyzed region, which represents almost twice the values recorded in any other year. Valle Seijo et al. (2024a) also noted a 113% increase in fire pixel counts for 2020 compared to the mean value observed in the broader study period (2013–2022).

The maximum FRP values were registered in 2020 and 2022, with median values of 5.95 MW and 6.3 MW, respectively, indicating periods of enhanced fire intensity. However, higher FRP or fire pixel counts do not necessarily translate into proportionally higher regional AOD, as MAIAC AOD represents spatially averaged aerosol conditions over the entire study area. Low AOD values in non-burning regions, together with atmospheric transport and dispersion, can reduce the regional median AOD. Furthermore, fire activity in 2020 was more evenly distributed throughout the year and across the study region, whereas in 2022 fires were largely concentrated during the summer months and primarily over Corrientes Province (Argentina), limiting their influence on the annual, regionally averaged AOD.

The persistent La Niña phenomenon, which lasted for three consecutive years between 2020 and 2022, likely exacerbated these conditions by intensifying drier weather patterns in the region. These conditions resulted from the combined influence of natural, decades-long precipitation variability and rising temperatures, making the region vulnerable to severe soil desiccation and widespread droughts. April 2020 marked a peak: more than 30% of central and eastern South America experienced negative soil moisture anomalies of more than two standard deviations (Geirinhas et al., 2023).

Fig. 2 presents the spatio-temporal distribution of AOD at 470 nm over the area of study (see Fig. 1) from 2018 to 2022. Fig. 2 (a) depicts the annual mean AOD, while Fig. 2 (b) illustrates the annual standard deviation (SD) of AOD. In the annual mean AOD maps, predominantly low values (represented in blue) are observed in the southern part of the region, whereas higher values (depicted in green and yellow) are concentrated in the northern area. This northern region is typically

Table 1
Annual fire pixel counts, FRP and AOD (470 nm) statistics in the region of interest from 2018 to 2022. The AOD values are based on MAIAC/MODIS data. The number of fire pixels and FRP values (in megawatts) are derived from VIIRS/NPP.

Year	N° of fire pixels (VIIRS/NPP)	FRP (VIIRS/NPP)			AOD 470 nm (MAIAC/MODIS)		
		Q1	Median	Q3	Q1 [IC 95%]	Median [IC 95%]	Q3 [IC 95%]
2018	196367	2.91	5.15	9.4	0.079 [0.074, 0.086]	0.106 [0.100, 0.110]	0.134 [0.130, 0.143]
2019	221884	2.90	5.25	10.0	0.079 [0.074, 0.084]	0.105 [0.100, 0.111]	0.144 [0.131, 0.156]
2020	***546893***	***3.08***	***5.95***	***11.8***	**0.087 [0.083, 0.097]**	***0.118 [0.112, 0.126]***	**0.169 [0.158, 0.193]**
2021	270603	2.85	5.54	11.0	0.078 [0.074, 0.082]	0.104 [0.099, 0.110]	0.137 [0.130, 0.144]
2022	310114	3.09	6.3	12.4	0.082 [0.078, 0.087]	0.115 [0.110, 0.120]	0.149 [0.143, 0.159]

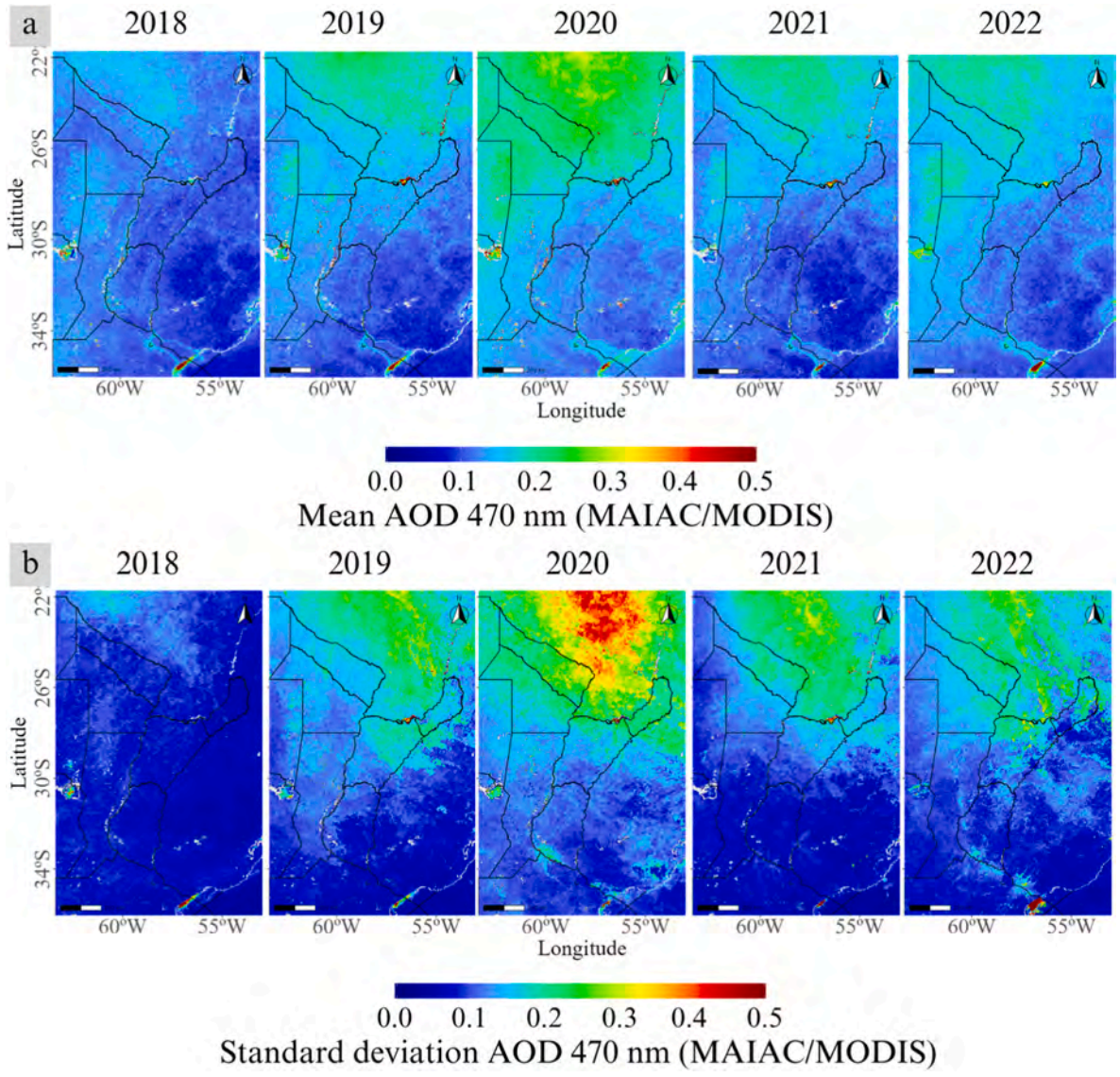

Fig. 2. Spatial distribution of AOD in southeastern South America from 2018 to 2022, derived from MAIAC/MODIS **(a)** Annual mean AOD (470 nm) **(b)** Annual standard deviation (SD) of AOD (470 nm). Note: values above 0.5 are shown in the same color. Maximum SD value observed in 2020 is 0.559. (For interpretation of the references to color in this figure legend, the reader is referred to the Web version of this article.)

associated with fire activity, particularly during the austral fire season, which occurs in the winter and spring months and significantly contributes to increase the aerosol load in the atmosphere (Martin et al., 2010). Previous studies have revealed that approximately 30% of the AOD in Paraguay and northern Argentina was associated with fires in the Amazon–Cerrado region (Castro Videla et al., 2013). Mulena et al. (2024) also found biomass-burning aerosols transported from Brazil over central Argentina during the period from July to December 2019.

Fig. 2 (a) shows consistently high AOD values over Mar Chiquita (Argentina), a saline lake located at approximately 30.7° S, 62.5° W (the large bluish object at the extreme left of Fig. 1c). A known limitation of the MAIAC algorithm is its difficulty in correctly identifying very bright, reflective surfaces such as saline lakes, which can lead to artificially high AOD values and missing surface retrievals. These high AOD values are possibly attributable to this known issue of the algorithm, as described by Lyapustin et al. (2018). Notably, these values were included in the statistics presented in Table 1, as this region represents only 0.5% of the total study area and affects the median by approximately ±0.0001.

The annual mean AOD values for 2018, 2019, and 2021 reflect relatively clean air conditions, while 2020 shows a marked increase in AOD, with substantial areas transitioning to the green and yellow color-scale values of Fig. 2 (a) (corresponding to mean AOD values above 0.2). This increase aligns with the surge in fire activity recorded that year, as shown in Table 1. The elevated AOD in Buenos Aires province (Argentina) and Uruguay during 2020 are very likely attributed to the transport of aerosols from biomass burning events occurring that year in northern regions.

By 2022, AOD values decreased relative to 2020 but remained higher than those observed in 2018 and 2019. Notably, during the summer of 2022, a significant number of fire events occurred in the northeastern region of Corrientes province located in Argentina (27.99° S, 57.02° W, refer to Fig. 1b). These fires caused the burning of almost 50% of the Iberá National Park (Smichowski & Contreras, 2024), contributing to elevated AOD, as reflected in the annual mean AOD map for that year.

Fig. 2 (b) highlights the annual variability in AOD values across the region each year. In 2020, the standard deviation reached its highest value, with red areas indicating substantial fluctuations in AOD values. This suggests the presence of episodic events, such as intense fire outbreaks, contributing to the variability. This is particularly evident along the southern border of Entre Ríos province in Argentina, where the

Paraná wetlands (32.89°S, 60.27°W, refer to Fig. 1b) experienced numerous fire events and extensive burned areas in 2020 (Del Valle et al., 2022).

In contrast, 2018 exhibited more stable and uniform conditions, as shown by predominantly blue areas in the standard deviation map. This lower variability is not only associated with a reduced number of fire events but also with a more evenly distributed temporal variation of these events. In 2019, 2021, and 2022, a moderate degree of variability was observed, particularly in the northern area. The presence of yellow and green regions in these years indicates ongoing fluctuations in aerosol emissions, probable linked to the usual fire season, which, as previously mentioned, typically occurs during the winter and spring months.

A higher degree of variability is observed in the northern region of Corrientes province (Argentina) in 2022 compared to other years. This increase in this area is likely related to the significant fire events that occurred during the summer of 2022, as mentioned earlier.

3.2. Seasonal variability of MAIAC/MODIS AOD

Seasonal variability offers insight into how biomass burning activity influences regional aerosol conditions. As summarized in Table 2, the study area shows clear seasonal contrasts in AOD, fire pixel density, and FRP between 2018 and 2022. Median summer AOD values remained relatively low from 2018 to 2021, ranging from 0.104 to 0.131, indicating generally clean atmospheric conditions. However, in 2022, the median AOD rose sharply to 0.163, coinciding with a significant increase in fire pixel counts (169,076, over five times higher than in 2021) and the highest FRP median value (7.26 MW). This analysis allows the proper characterization of the intense fire events that occurred in the Corrientes province (Argentina) during the summer of 2022, as mentioned above.

Median AOD values during autumn remained consistently low across all years, fluctuating slightly around 0.09 to 0.11. However, 2020 stands out with an extraordinary fire pixel count of 110,380, nearly ten times greater than the mean for other years in this season. During autumn 2020, the FRP remained relatively stable compared to other seasons (e.g., summer 2022). This suggests that, although the number of fire pixels was high, the fire intensity was moderate. Consequently, it is likely that this high fire pixel count did not lead to a proportional increase in the median AOD. A specific study analyzing data from March 2017 to March 2023 for Rosario city, Argentina (32.95° S, 60.63° W) revealed that during wildfire events, such as in March 2023, AOD surged by approximately 50.9% to 108.6% compared to the business-as-usual scenarios observed in March 2019 and March 2022, respectively (Valle Seijo et al., 2024b).

The highest median AOD value (0.116) was recorded for winter 2021. Although it did not register the highest number of fire pixels, it recorded an elevated median FRP (5.72 MW) underscoring a link between fire intensity and AOD values. Additionally, winter 2020 showed the highest fire pixel counts (202,242), which corresponded with an elevated AOD value (0.114). These findings emphasize the significant contribution of biomass burning during the austral winter to regional aerosol loading.

In general, spring showed the highest median AOD values of all seasons, revealing the culmination of the austral fire season. The year 2020 had the highest median AOD (0.154) and fire pixel count (200,204), along with the highest median FRP (6.32 MW). These patterns are surely a direct consequence of the findings by Ulke et al. (2011), who documented the role of meteorological conditions, such as the South American Low-Level Jet and cold front dynamics, in modulating the dispersion and transport of regional smoke plumes.

To examine intraseasonal differences in fire season, monthly fire pixel counts are shown in Fig. S3. In 2020, fire activity began to increase earlier than in other years, with increased fire numbers already observed in June and July, followed by a pronounced peak in August and continued activity until October. This indicates that the 2020 fire season started earlier and lasted longer than in most other years. The particularly high values of the variables analyzed in Table 2 for winter and spring of 2020–2021 prompted the inclusion of Fig. 3 in this study to examine the spatial distribution of AOD values in greater detail.

Focusing on the winter season, the mean AOD during the winter of 2020 (Fig. 3a) indicates moderate values in the northern regions, with green and yellow areas showing AODs above 0.2, particularly in fire-prone areas such as Paraguay and northern Argentina (refer to Fig. S2 to see density maps of the spatial distribution of fire pixels). In contrast, the AODs of winter 2021 exhibit broader spatial coverage, especially in the northern half of the region, where AOD values consistently exceed 0.2. The springtime (2020 and 2021) standard deviation AOD maps (Fig. 3b) highlight greater variability in fire-prone areas, suggesting episodic fire events, while southern regions display more uniform conditions with reduced variability. One notable exception is the Paraná River wetlands, located approximately at 32.89° S and 60.27° W, which, as discussed in Section 3.1, also recorded a higher number of fire pixels during 2020.

The spring 2020 mean AOD map reveals extensive red and orange regions, indicating significant aerosol loading, particularly in northern Paraguay, northern Argentina, and parts of Brazil, with values exceeding 0.5. These elevated values align with the record-breaking fire activity and emissions observed that year (Fig. S2). Spring 2021 shows similar patterns with high AODs extending over a slightly reduced area. Variability in spring 2020 and spring 2021 (Fig. 3b) is particularly pronounced, again reflecting the intensity and irregularity of biomass burning events.

Table 2
Seasonal variation of AOD (470 nm), fire pixel counts, and FRP in the region of interest from 2018 to 2022. The data is presented for each season (summer, autumn, winter, spring). Data source: MAIAC/MODIS data.

Season	Variable	Year				
		2018	2019	2020	2021	2022
Summer	Median AOD [IC 95%]	0.131 [0.121–0.139]	0.108 [0.100–0.120]	0.130 [0.116–0.149]	0.104 [0.095–0.115]	0.163 [0.145–0.189]
	N° of fire pixels	32167	22557	32754	24276	169076
	Median FRP (MW)	5.12	5.04	5.10	4.89	7.26
Autumn	Median AOD [IC 95%]	0.098 [0.089–0.107]	0.088 [0.082–0.097]	0.092 [0.084–0.110]	0.089 [0.080–0.099]	0.108 [0.098–0.115]
	N° of fire pixels	31276	11774	110380	27701	22760
	Median FRP (MW)	4.92	4.49	5.68	4.58	4.64
Winter	Median AOD [IC 95%]	0.082 [0.072–0.091]	0.094 [0.085–0.112]	***0.114 [0.104–0.121]***	***0.116 [0.096–0.123]***	0.114 [0.094–0.124]
	N° of fire pixels	90398	76972	***202242***	***131917***	59147
	Median FRP (MW)	5.31	4.80	***5.97***	***5.72***	5.50
Spring	Median [IC 95%]	0.116 [0.097–0.131]	0.127 [0.112–0.158]	***0.154 [0.130–0.196]***	***0.138 [0.123–0.167]***	0.101 [0.089–0.118]
	N° of fire pixels	48809	108421	***200204***	***67027***	74125
	Median FRP (MW)	5.17	5.79	***6.32***	***5.60***	5.50

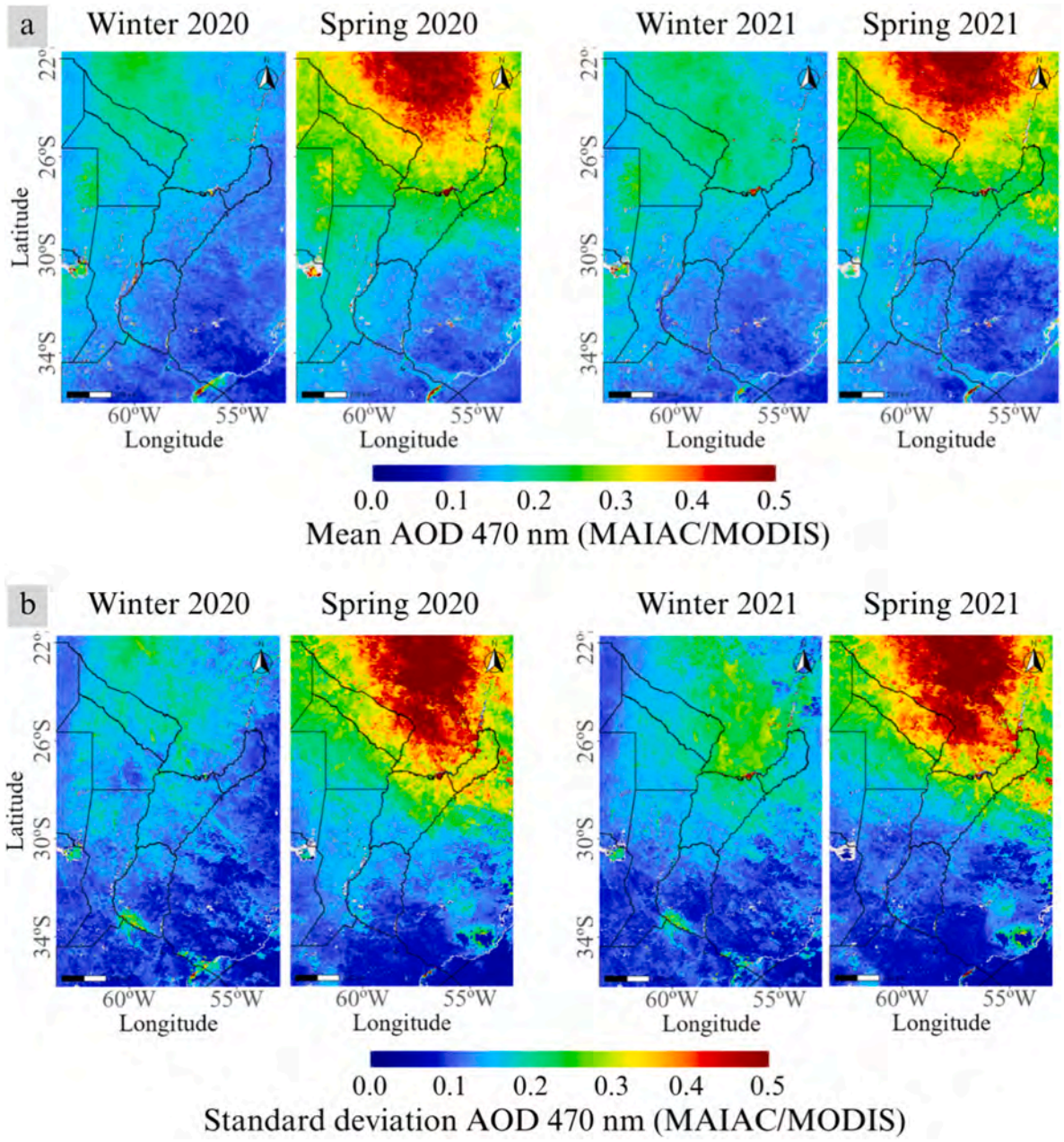

Fig. 3. Spatial distribution of AOD over southeastern South America during winter and spring seasons of 2020 and 2021, based on MAIAC/MODIS data. **(a)** Seasonal mean AOD (470 nm) **(b)** Seasonal standard deviation (SD) of AOD (470 nm). Maximum mean AOD was 0.642 and maximum SD was 0.662 in spring 2020; maximum mean was 0.607 and maximum SD was 0.648 in spring 2021.

3.3. Evaluation of MAIAC performance at two urban sites in southeastern South America

Heterogeneous land surfaces, such as urban areas, can introduce uncertainties in MAIAC AOD retrievals (Martins et al., 2017). Consequently, understanding how these surface characteristics vary across the study region is essential for interpreting the agreement between satellite and in-situ observations. Table 3 provides a comparative analysis of land cover distribution throughout the total study area and the surroundings of AERONET stations in Buenos Aires (CEILAP) and Montevideo. The land cover data were obtained from the CGLS-LC100 product at a 100 m spatial resolution (section 2.1). A 25 × 25 km^2 buffer area was selected to characterize land cover over the two AERONET stations. The table reveals significant discrepancies between the total study area and the land covers surrounding these AERONET stations.

The total study area primarily consists of cropland, forest, savanna, and grassland covers, comprising 82.6% of the total. A study validating the MAIAC product over South America (Martins et al., 2017) reported high-confidence retrievals over these land cover types, with more than approximately 66% of the retrievals falling within the expected error (Equation (1)) and a Pearson correlation coefficient exceeding 0.86. Similar studies conducted in other parts of the world have also demonstrated a strong correlation between MAIAC and AERONET observations over these land cover types (Mhawish et al., 2019; Superczynski et al., 2017; Zhang et al., 2019).

Urban land covers account for only 0.5% of the total study area but constitute 48% and 10.7% around the buffer areas surrounding the Buenos Aires and Montevideo AERONET stations. This urban dominance introduces unique challenges for MAIAC retrievals, as urban areas often feature highly reflective surfaces (e.g., concrete and asphalt). These

Table 3
Comparison of land cover percentages across the total study area and corresponding observations from AERONET stations (25 × 25 km^2 buffer area) in Buenos Aires (CEILAP) and Montevideo. Data source: CGLS-LC100 product at 100 m spatial resolution.

Land cover	Total Area of study (%)	AERONET Buenos Aires (CEILAP) (%)	AERONET Montevideo (%)
Savanna/ Grassland	30.8	12	20.0
Forest	28.5	4.3	3.9
Cropland	23.3	1.7	1.9
Herbaceous wetland	6.7	2.4	1.5
Open Water	5.1	29.9	61.2
Shrubland/ Barren	3.3	1.1	0.2
Permanent waterbodies	1.7	0.4	0.5
Urban/built up	0.5	48.0	10.7

complex urban areas contribute significantly to the top of atmosphere reflectance, which diminishes the sensitivity of aerosol measurements (Martins et al., 2017).

Fig. 4 compares MAIAC/MODIS AOD at 470 nm with AERONET AOD at 440 nm for Buenos Aires and Montevideo. Data from both Aqua and Terra satellites are presented in separate panels. Key statistical metrics are displayed for each comparison (see equations from section 2.4.1): the number of data points (N), correlation coefficient (R), root mean square error (RMSE), bias, and the percentage of points falling within the MAIAC expected error (EE).

The number of data points between Buenos Aires and Montevideo differs due to the lesser availability of Montevideo data, which can constrain conclusions about long-term trends and reduce the robustness of statistical comparisons. Scatter plots showed correlation coefficients of approximately 0.7 for Aqua at both sites, with slightly lower coefficients for Terra. However, a Fisher's z-test indicated that the difference between satellites was statistically significant only in Montevideo ($z = 2.81$, $p = 0.002$, $\alpha = 0.05$). Martins et al. (2017) reported similar R values (0.636 for Aqua and 0.686 for Terra) for urban sites, including São Paulo and Buenos Aires.

RMSE values, ranging from 0.069 to 0.089, indicate moderate variability. The bias is relatively small for moderate to high AODs (e.g., during smoke events with AODs >0.5) but may be more significant for lower AOD values. Notably, a higher percentage of points falls within the expected error for Aqua data (63.53–72.22%) compared to Terra data (62.25–68.24%). Martins et al. (2017) showed similar results when they concluded that AQUA observations are more appropriate for urban observations. The 1:1 line (black) and the shaded gray area representing the expected error boundaries provide a visual reference for assessing the agreement between the datasets.

3.4. MAIAC correlation with AERONET observations during fire events

The accuracy of MAIAC is influenced not only by its dependence on land cover as evaluated thus far, but also by additional factors such as AOD magnitude, aerosol size, and seasonal variations (Zhang et al., 2019). Stronger correlations between MAIAC and AERONET are expected during fire seasons or years of significant fire activity, like 2020 (Daniels et al., 2024). This is because the increased aerosol load from fires tends to dominate the signal, potentially reducing the influence of land cover type on retrieval accuracy and improving the alignment between satellite and ground-based observations.

Assessing the correlation between AOD values from MAIAC/MODIS and AERONET during fire seasons helps determine whether fires in the northern part of the study area impacted Buenos Aires and Montevideo,

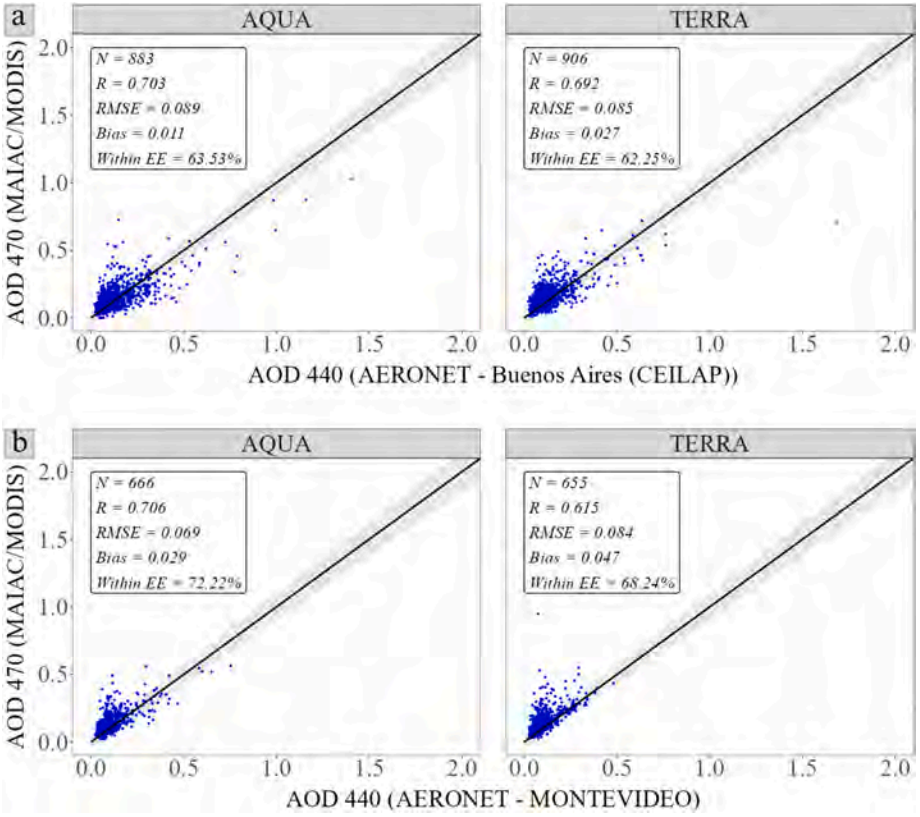

Fig. 4. Scatter plots of MAIAC/MODIS AOD 470 nm compared with AERONET AOD 440 nm at **(a)** Buenos Aires-CEILAP (2018–2022) and **(b)** Montevideo (2020–2022). Both Aqua and Terra satellite data are included. The black line represents the 1:1 relationship and the shaded gray area represent MAIAC expected error (refer to Equation (1)).

both located in the south. Given the challenges of satellite-based AOD retrievals in urban areas, we anticipate stronger correlations during fire seasons, which would indicate that the fires influenced air quality in these cities.

In the supplementary material, Table S1 summarizes the performance of MAIAC AODs during winter and spring at the AERONET sites. The table also shows the seasonal results reported by Martins et al. (2017). Winter and spring are considered the fire season in this region as described in Section 3.2. Overall, the data revealed moderately strong correlations (R close to 0.7-0.8) between MAIAC and AERONET AOD at both Buenos Aires and Montevideo. In Buenos Aires, the seasonal correlations for winter and spring exceeded the overall correlations for the entire period (R for Terra = 0.69 and R for Aqua = 0.70). However, when applying Fisher's *z*-transformation, only the Terra observations showed a statistically significant difference for this comparison (refer to Table S2).

In Montevideo, the seasonal correlations for winter and spring also exceeded the overall values (R for Terra = 0.62 and R for Aqua = 0.71). In this case, Fisher's *z*-test indicated that a statistically significant difference was present only for the winter observations (Table S2).

Finally, when comparing seasonal results with those reported by Martins et al. (2017), this study showed generally higher performance across all metrics (Table S1). This may indicate that recent fires exerted a greater influence on aerosol values. However, since Martins et al. (2017) did not report the number of data points, it was not possible to evaluate the statistical significance of the correlation coefficient comparisons.

Table S2 compares correlations during winter and spring (Table S1) with those calculated for the entire study period (Fig. 4). It is important to note that the full-period dataset used in Fig. 4 already included the fire seasons. Consequently, this may explain why some of the observed differences in correlations were not statistically significant.

To better capture the possible impact of fire events on air quality in Buenos Aires and Montevideo, we also analyzed the year-by-year correlations between MAIAC and AERONET AOD. As highlighted in Section 3.1, 2020 was an exceptional year, characterized by a significant surge in fire activity. A total of 546,893 fire pixels were detected—more than double the values recorded in any other year—and median FRP reached

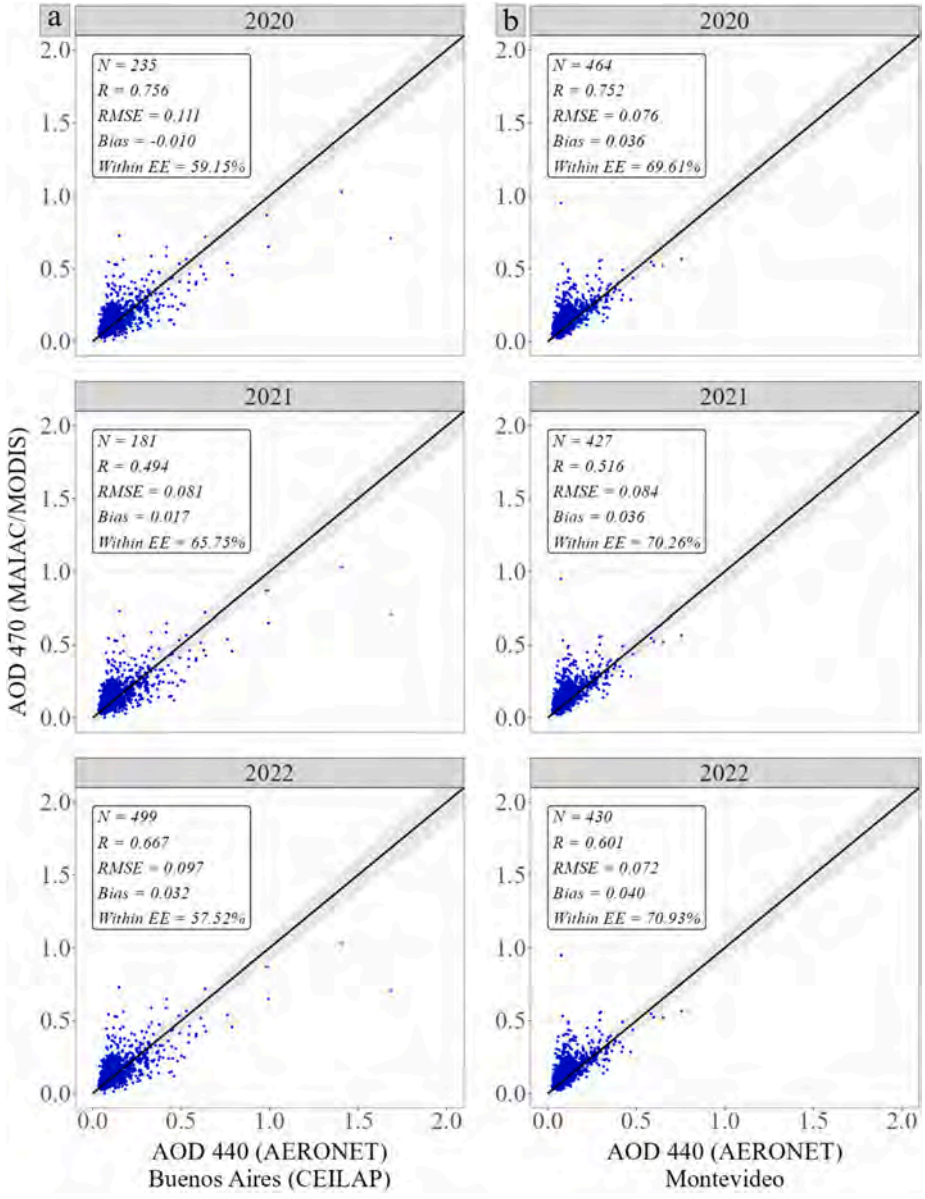

Fig. 5. Yearly scatter plots comparing satellite (MAIAC/MODIS) and AERONET AOD for 2020–2022 at **(a)** Buenos Aires-CEILAP and **(b)** Montevideo. The 1:1 line and MAIAC expected error are indicated (refer to Equation (1)).

its highest value at 6.32 MW.

Fig. 5 presents yearly scatter plots for 2020, 2021, and 2022 at the two locations, comparing MAIAC/MODIS AOD with AERONET AOD. The plots include data from both Aqua and Terra satellites and the same statistics reported in Fig. 4.

As with seasonal results, AERONET observations exhibited moderately strong correlations with MAIAC AOD in 2020 (R close to 0.75). However, in this case, Fisher's z-tests indicated statistically significant differences when comparing correlations with years that had fewer fire events. In Buenos Aires, the correlation in 2020 was significantly higher than in 2021 ($z = 4.47$, $p < 0.001$) and 2022 ($z = 2.28$, $p = 0.01$). In Montevideo, the 2020 correlation was significantly greater than in 2021 ($z = 6.04$, $p < 0.001$) and 2022 ($z = 4.21$, $p < 0.001$). Overall, Montevideo showed a higher percentage of data falling within the expected error, which may be attributed to its lower proportion of land classified as urban (See Table 3). This reduced urban coverage likely minimized challenges associated with MAIAC retrievals over highly reflective urban surfaces, contributing to the improved accuracy observed in Montevideo.

3.5. Correlation between AE and AOD during biomass burning events at AERONET sites

The Ångström Exponent provides insights into particle size and composition, especially for aerosols generated by biomass burning (Eck et al., 1999). These aerosols are primarily composed of black carbon and brown carbon, which have distinct absorption characteristics that affect the AE (Tuccella et al., 2025). Emissions from biomass burning result in aerosol absorption values in South America being approximately ten times higher during the dry season than during the rainy season (Rizzo et al., 2011).

Fig. 6 shows scatter plots of the relationship between AE and AOD (440 nm) for the Buenos Aires and Montevideo AERONET stations. At both stations, AE variability was indicative of differences in aerosol particle size and source composition. The left plot of Fig. 6 (a) depicts winter 2020 (red dots) in comparison to other winter seasons (light red dots) and other seasons (gray dots). The right plot shows similar data for spring 2020 (green dots) compared to other spring seasons (light green dots) and other seasons (gray dots). Aerosol optical depth values for Buenos Aires were typically between 0 and 1.5, with AE values exceeding 1.0 in many cases: this shows the dominance of fine-mode aerosols that are likely associated with biomass burning or urban pollution. Fig. 6 (b) illustrates the same relationships for the Montevideo station. This station exhibits AOD values between 0 and 1.0.

In Buenos Aires, winter 2020 exhibited a notable shift in the AOD-AE relationship compared to previous winters (larger AOD values for similar AE ranges). This shift is indicative of increased aerosol loading and potential changes in aerosol optical properties. The spring 2020

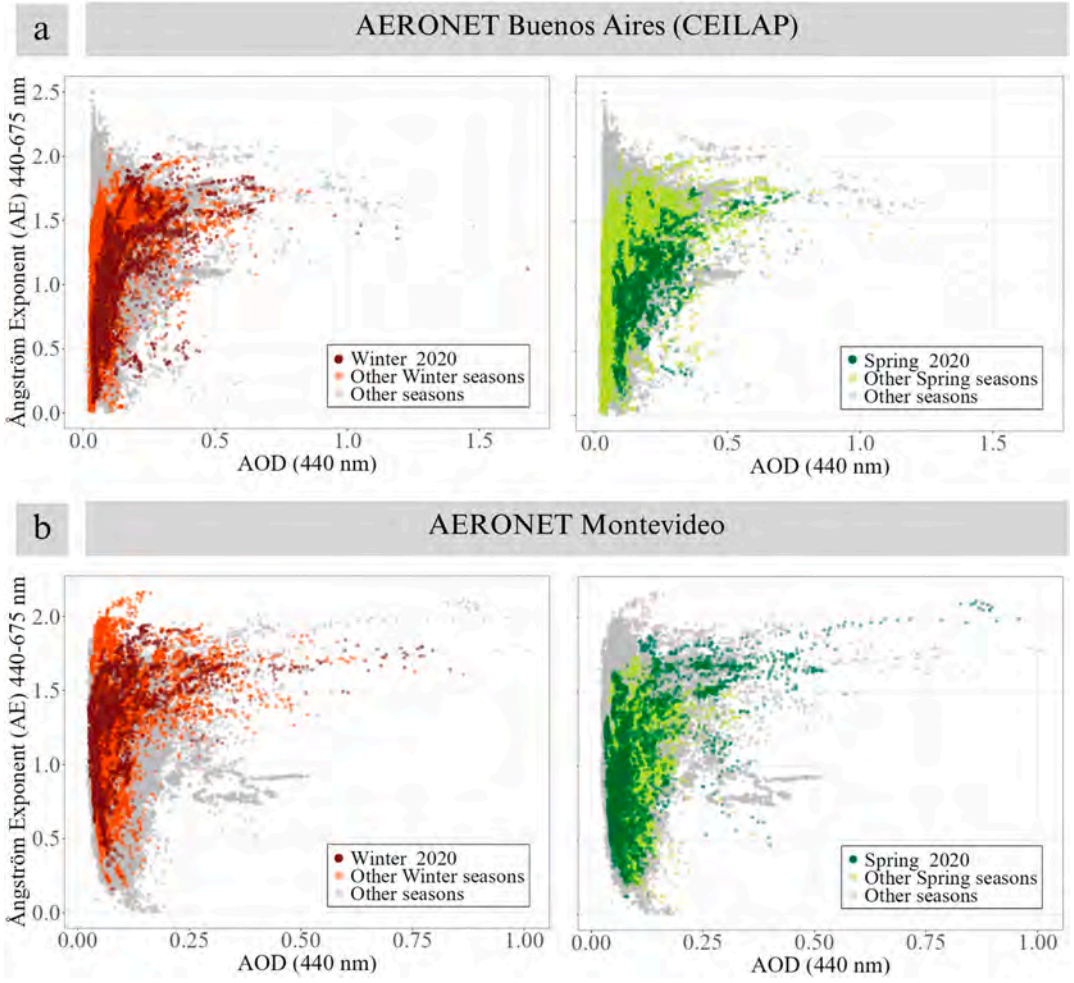

Fig. 6. Scatter plots showing the relationship between AOD at 440 nm and AE 440–675 nm for AERONET stations at **(a)** Buenos Aires (CEILAP) and **(b)** Montevideo. Data are highlighted for winter 2020 (dark red) and spring 2020 (dark green). Other highlighted seasons include data from 2018 to 2022 for Buenos Aires and 2021–2022 for Montevideo. Points depicted in gray correspond to data from seasons other than the theme season (winter or spring) of a given scatter plot. Note: The data record for Montevideo (2020–2022) is shorter than that for Buenos Aires (2018–2022). (For interpretation of the references to color in this figure legend, the reader is referred to the Web version of this article.)

data showed a similar pattern. In Montevideo, no significant shift was observed, possibly due to the limited length of the data record. Seasonal patterns remained consistent, with AE values mostly ranging between 1 and 2 during winter. There was a notably greater proportion of data with AE values exceeding 1.5 in the spring of 2020. This could be related to specific days when aerosols from biomass burning reached Montevideo.

These observations corroborated the seasonal analysis presented earlier, where AE values between 1 and 2 were linked to biomass burning emissions. The data also highlighted the episodic nature of biomass burning plumes and their ability to significantly impact aerosol loading and properties in distant areas (refer to Fig. S2). These findings are consistent with previous assessments for Montevideo (Osorio et al., 2024) and Buenos Aires (Otero et al., 2020; Otero et al., 2013; Ulke et al., 2011).

Biomass burning and urban aerosols may exhibit similar AE values, depending on particle size distribution and aging processes. The inclusion of aerosol inversion products from AERONET can improve aerosol type discrimination. However, previous studies have shown that, in South America, there are no AERONET sites with consistently high AOD values, which significantly limits the availability of reliable inversion products (Hamill et al., 2016). Consequently, this constraint makes it unfeasible to comprehensively classify aerosol types using inversion products alone, as also discussed by Scagliotti et al. (2024).

Despite the general scarcity of inversion data, single scattering albedo (SSA) retrievals were available on two days in 2020 at both the Buenos Aires and Montevideo AERONET stations, which are worth discussing as illustrative case studies. At the Buenos Aires site, on August 3, 2020, SSA values ranged from 0.87 to 0.90 between 15:00 and 19:00 local time. During this period, AOD increased from values close to 0.2 to approximately 0.65, while AE values remained close to 1.0. Another retrieval occurred on 18 August 2020, with SSA values between 0.84 and 0.87 around 18:00 local time, accompanied by AOD values close to 1.0 and AE values near 1.2.

At the Montevideo station, SSA values on 5 August 2020 ranged from 0.92 to 0.93 between 18:00 and 19:00 local time. During this interval, AOD increased from approximately 0.2 to about 0.75, while AE values were close to 1.5. On 18 August 2020, an SSA value of approximately 0.88 was retrieved at 18:00 local time, with AOD remaining near 0.5 and AE close to 1.4.

Previous studies focusing on aerosol classification indicate that biomass-burning aerosols are typically characterized by SSA values ranging from 0.85 to 0.92, owing to the presence of internally mixed black carbon and organic carbon (Li et al., 2022; Devi and Satheesh, 2022c). Measurements conducted in South America have shown that biomass-burning aerosols in Amazonia exhibit SSA values ranging from approximately 0.81 to 0.94, derived from irradiance measurements combined with aerosol optical properties and cloudless-sky radiative transfer models (Eck et al., 1998). Other studies report SSA values between 0.8 and 0.9 during the dry season, when biomass-burning activity is strongest in South America, and values exceeding 0.9 during the wet season (Takemura et al., 2002).

To further reinforce the interpretation of the observed aerosol optical properties, HYSPLIT backward air-mass trajectory analyses were performed for the days with available SSA retrievals and are included in the Supplementary Material (refer to Fig. S4). These trajectories indicate that the air masses reaching both Buenos Aires and Montevideo originated from northern regions of South America, where active biomass-burning episodes were occurring during the study period. This transport pathway supports the attribution of the observed moderate SSA values and enhanced AOD to the influence of biomass-burning aerosols, despite the limited availability of inversion products.

4. Conclusions

This study presents an integrated analysis of MAIAC/MODIS aerosol products, VIIRS fire detections, and AERONET observations over southeastern South America. During 2020, wildfire detections increased by approximately 119% relative to adjacent years, while annual median satellite AOD increased by about 10% with respect to the baseline of the same period. Although the largest impacts are observed over rural and fire-prone areas, the results show that wildfire emissions can extend well beyond source regions and affect major urban centers, including Buenos Aires and Montevideo.

The statistically significant higher correlations between satellite derived AOD and ground-based observations during 2020 indicate that MAIAC retrievals are particularly robust under smoke conditions, even over complex urban surfaces. This finding supports the use of high-resolution satellite products during wildfire episodes, when accurate monitoring is most critical.

By incorporating AERONET observations from Montevideo for the first time into the validation of MAIAC products, this work strengthens confidence in satellite-based aerosol assessments across southern South America. The results provide a basis for future studies aimed at expanding satellite aerosol validation under biomass-burning events, particularly over complex urban surfaces and coastal regions. Continued use of AERONET observations would help identify retrieval strengths and limitations during extreme events and guide the refinement of satellite aerosol products for regional applications.

CRediT authorship contribution statement

María Fernanda Valle Seijo: Writing – review & editing, Writing – original draft, Visualization, Validation, Software, Methodology, Investigation, Formal analysis, Data curation, Conceptualization. **Lidia Ana Otero:** Writing – review & editing, Supervision, Resources, Project administration, Funding acquisition, Formal analysis, Conceptualization. **Alejandro Agesta:** Writing – review & editing, Resources, Conceptualization. **Erna Frins:** Writing – review & editing, Supervision, Resources, Project administration, Conceptualization. **Rubén Darío Piacentini:** Writing – review & editing, Supervision, Project administration, Funding acquisition, Conceptualization.

Declaration of competing interest

The authors declare that they have no known competing financial interests or personal relationships that could have appeared to influence the work reported in this paper.

Acknowledgments

We acknowledge the mission scientists and Principal Investigators who provided the data used in this research effort. M. Fernanda Valle Seijo expresses gratitude to the Consejo Nacional de Investigaciones Científicas y Técnicas (CONICET) for its support. Alejandro Agesta thanks the support received by the Agencia Nacional de Investigación e Innovación (ANII), grant no. POS_NAC_2022_1_174198 and the Comisión Académica de Posgrado (UDELAR), grant no. BDDX_2024_1#49154935. Erna Frins thanks the Programa de Desarrollo de Ciencias Básicas (PEDECIBA, Uruguay) for its support.

Appendix A. Supplementary data

Supplementary data to this article can be found online at https://doi.org/10.1016/j.envpol.2026.127940.

Data availability

The MCD19A2 V.6.1 product (Lyapustin and Wang, 2022), used for satellite-based AOD characterization in this study, is available at NASA Earthdata Search (Earthdata Search, 2019) via https://earthdata.nasa.gov/. Ground-based AOD data were obtained from AERONET using its web download tool (https://aeronet.gsfc.nasa.gov/). The software

(v1.0.0), which includes the code used for data analysis and visualization in this work, is preserved on Zenodo (https://doi.org/10.5281/zenodo.14740511) under the GPL 3.0 license. It is openly developed on GitHub at https://github.com/Fernandavalleseijo/AOD_MAIAC-MODIS_AERONET (Valle Seijo, 2025).

References

Abuelgasim, A., Bilal, M., Alfaki, I.A., 2021. Spatiotemporal variations and long term trends analysis of aerosol optical depth over the United Arab Emirates. Remote Sens. Appl.: Soc. Environ. 23, 100532. https://doi.org/10.1016/j.rsase.2021.100532.

Apte, J.S., Manchanda, C., 2024. High-resolution urban air pollution mapping. Science 385 (6707), 380–385. https://doi.org/10.1126/science.adq3678.

Barreto, Á., Cuevas, E., Granados-Muñoz, M.-J., Alados-Arboledas, L., Romero, P.M., Gröbner, J., Kouremeti, N., Almansa, A.F., Stone, T., Toledano, C., Román, R., Sorokin, M., Holben, B., Canini, M., Yela, M., 2016. The new sun-sky-lunar Cimel CE318-T multiband photometer – a comprehensive performance evaluation. Atmos. Meas. Tech. 9 (2), 631–654. https://doi.org/10.5194/amt-9-631-2016.

Bolaño-Diaz, S., Camargo-Caicedo, Y., Tovar Bernal, F., Bolaño-Ortiz, T.R., 2022. The effect of forest fire events on air quality: a case study of Northern Colombia. Fire 5 (6), 191. https://doi.org/10.3390/fire5060191.

Brauer, M., et al., 2024. Global burden and strength of evidence for 88 risk factors in 204 countries and 811 subnational locations, 1990- 2021: a systematic analysis for the global burden of disease study 2021. Lancet 403 (10440), 2162–2203. https://doi.org/10.1016/S0140-6736(24)00933-4.

Buchhorn, M., Lesiv, M., Tsendbazar, N.-E., Herold, M., Bertels, L., Smets, B., 2020. Copernicus global land cover layers—collection 2. Remote Sens. 12 (6), 1044. https://doi.org/10.3390/rs12061044.

Castro Videla, F., Barnaba, F., Angelini, F., Cremades, P., Gobbi, G.P., 2013. The relative role of Amazonian and non-Amazonian fires in building up the aerosol optical depth in South America: a five year study (2005–2009). Atmos. Res. 122, 298–309. https://doi.org/10.1016/j.atmosres.2012.10.026.

Christopher, S., Gupta, P., 2020. Global distribution of column satellite aerosol optical depth to surface $PM_{2.5}$ relationships. Remote Sens. 12 (12), 1985. https://doi.org/10.3390/rs12121985.

Chu, D.A., Kaufman, Y.J., Ichoku, C., Remer, L.A., Tanré, D., Holben, B.N., 2002. Validation of MODIS aerosol optical depth retrieval over land. Geophys. Res. Lett. 29 (12). https://doi.org/10.1029/2001GL013205.

Cobelo, I., Castelhano, F.J., Borge, R., Roig, H.L., Adams, M., Amini, H., Koutrakis, P., Réquia, W.J., 2023. The impact of wildfires on air pollution and health across land use categories in Brazil over a 16-year period. Environ. Res. 224, 115522. https://doi.org/10.1016/J.ENVRES.2023.115522.

Daniels, J., Liang, L., Benedict, K.B., Brahney, J., Rangel, R., Weathers, K.C., Ponette-González, A.G., 2024. Satellite-based aerosol optical depth estimates over the continental U.S. during the 2020 wildfire season: roles of smoke and land cover. Sci. Total Environ. 921, 171122. https://doi.org/10.1016/j.scitotenv.2024.171122.

Del Valle, H., Sione, W.F., Aceñolaza, P.G., 2022. Wetland fire assessment and monitoring in the Paraná River Delta, using radar and optical data for burnt area mapping. Fire 5 (6), 190. https://doi.org/10.3390/fire5060190.

Devi, A., Satheesh, S.K., 2022. Global maps of aerosol single scattering albedo using combined CERES-MODIS retrieval. Atmos. Chem. Phys. 22 (8), 5365–5376. https://doi.org/10.5194/acp-22-5365-2022.

Earthdata Search, 2019. Greenbelt, MD: Earth Science Data and Information System (ESDIS) Project, Earth Science Projects Division (ESPD). Flight Projects Directorate, Goddard Space Flight Center (GSFC) National Aeronautics and Space Administration (NASA). URL. https://search.earthdata.nasa.gov/.

Eck, T.F., Holben, B.N., Slutsker, I., Setzer, A., 1998. Measurements of irradiance attenuation and estimation of aerosol single scattering albedo for biomass burning aerosols in Amazonia. J. Geophys. Res. Atmos. 103 (D24), 31865–31878. https://doi.org/10.1029/98jd00399.

Eck, T.F., Holben, B.N., Reid, J.S., Dubovik, O., Smirnov, A., O'Neill, N.T., S, I., Kinne, S., 1999. Wavelength dependence of the optical depth of biomass burning, urban, and desert dust aerosols. J. Geophys. Res. Atmos. 104 (D24), 31333–31349. https://doi.org/10.1029/1999JD900923.

Fathollahi, L., Wu, F., Maleki, R., Pongracic, B., 2023. $PM_{2.5}$ concentrations estimation using machine learning methods with combination of MAIAC - MODIS AOD product - a case study in Western Iran. Air Qual. Atmos. Health 16 (8), 1529–1541. https://doi.org/10.1007/s11869-023-01354-9.

Fisher, R.A., 1915. Frequency distribution of the values of the correlation coefficient in samples from an indefinitely large population. Biometrika 10 (4), 507. https://doi.org/10.2307/2331838.

Gao, Y., Huang, W., Yu, P., Xu, R., Yang, Z., Gasevic, D., Ye, T., Guo, Y., Li, S., 2023. Long-term impacts of non-occupational wildfire exposure on human health: a systematic review. Environ. Pollut. 320, 121041. https://doi.org/10.1016/J.ENVPOL.2023.121041.

Garcia, L.C., et al., 2021. Record-breaking wildfires in the world's largest continuous tropical wetland: integrative fire management is urgently needed for both biodiversity and humans. J. Environ. Manag. 293, 112870. https://doi.org/10.1016/j.jenvman.2021.112870.

Geirinhas, J.L., Russo, A.C., Libonati, R., Miralles, D.G., Ramos, A.M., Gimeno, L., Trigo, R.M., 2023. Combined large-scale tropical and subtropical forcing on the severe 2019–2022 drought in South America. npj Clim. Atmos. Sci. 6 (1), 185. https://doi.org/10.1038/s41612-023-00510-3.

Giles, D.M., Sinyuk, A., Sorokin, M.G., Schafer, J.S., Smirnov, A., Slutsker, I., Eck, T.F., Holben, B.N., Lewis, J.R., Campbell, J.R., Welton, E.J., Korkin, S.V., Lyapustin, A.I., 2019. Advancements in the aerosol robotic network (AERONET) version 3 database – automated near-real-time quality control algorithm with improved cloud screening for Sun photometer aerosol optical depth (AOD) measurements. Atmos. Meas. Tech. 12 (1), 169–209. https://doi.org/10.5194/amt-12-169-2019.

Guerrero, F., Espinoza, L., Vidal, V., Carmona, C., Krecl, P., Targino, A.C., Ruggeri, M.F., Toledo, M., 2024. Black carbon and particulate matter concentrations amid central Chile's extreme wildfires. Sci. Total Environ. 951, 175541. https://doi.org/10.1016/J.SCITOTENV.2024.175541.

Holben, B.N., Eck, T.F., Slutsker, I., Tanré, D., Buis, J.P., Setzer, A., Vermote, E., Reagan, J.A., Kaufman, Y.J., Nakajima, T., Lavenu, F., Jankowiak, I., Smirnov, A., 1998. AERONET—A federated instrument network and data archive for aerosol characterization. Rem. Sens. Environ. 66 (1), 1–16. https://doi.org/10.1016/S0034-4257(98)00031-5.

Holben, B.N., Tanré, D., Smirnov, A., Eck, T.F., Slutsker, I., Abuhassan, N., Newcomb, W. W., Schafer, J.S., Chatenet, B., Lavenu, F., Kaufman, Y.J., Castle, J. Vande, Setzer, A., Markham, B., Clark, D., Frouin, R., Halthore, R., Karneli, A., O'Neill, N.T., et al., 2001. An emerging ground-based aerosol climatology: aerosol optical depth from AERONET. J. Geophys. Res. Atmos. 106 (D11), 12067–12097. https://doi.org/10.1029/2001JD900014.

Huang, W., Xu, H., Wu, J., Ren, M., Ke, Y., Qiao, J., 2024. Toward cleaner air and better health: current state, challenges, and priorities. Science 385 (6707), 386–390. https://doi.org/10.1126/science.adp7832.

Ichoku, C., Chu, D.A., Mattoo, S., Kaufman, Y.J., Remer, L.A., Tanré, D., Slutsker, I., Holben, B.N., 2002. A spatio-temporal approach for global validation and analysis of MODIS aerosol products. Geophys. Res. Lett. 29 (12). https://doi.org/10.1029/2001GL013206.

Kaufman, Y.J., Tanré, D., Boucher, O., 2002. A satellite view of aerosols in the climate system. Nature 419 (6903), 215–223. https://doi.org/10.1038/nature01091.

Krecl, P., Oukawa, G.Y., Mollinedo Veneros, E.M., Targino, A.C., 2025. South America is on fire: an urgent call for national and regional actions. ACS ES&T Air 2 (1), 1–3. https://doi.org/10.1021/acsestair.4c00251.

Lee, J., Kim, J., Song, C.H., Kim, S.B., Chun, Y., Sohn, B.J., Holben, B.N., 2010. Characteristics of aerosol types from AERONET sunphotometer measurements. Atmos. Environ. 44 (26), 3110–3117. https://doi.org/10.1016/j.atmosenv.2010.05.035.

Lei, Y., Lei, T.-H., Lu, C., Zhang, X., Wang, F., 2024. Wildfire smoke: health effects, mechanisms, and mitigation. Environ. Sci. Technol. https://doi.org/10.1021/acs.est.4c06653.

Li, Y., Yuan, S., Fan, S., Song, Y., Wang, Z., Yu, Z., Yu, Q., Liu, Y., 2021. Satellite remote sensing for estimating $PM_{2.5}$ and its components. Curr. Pollut. Rep. 7 (1), 72–87. https://doi.org/10.1007/s40726-020-00170-4.

Li, J., Carlson, B.E., Yung, Y.L., et al., 2022. Scattering and absorbing aerosols in the climate system. Nat. Rev. Earth Environ. 3, 363–379. https://doi.org/10.1038/s43017-022-00296-7.

Lyapustin, A., Wang, Y., 2022. *MODIS/Terra+Aqua Land Aerosol Optical Depth Daily L2G Global 1km SIN Grid V061* [Data set]. NASA EOSDIS Land Processes Distributed Active Archive Center. https://doi.org/10.5067/MODIS/MCD19A2.061. (Accessed 24 January 2025).

Lyapustin, A., Wang, Y., Laszlo, I., Kahn, R., Korkin, S., Remer, L., Levy, R., Reid, J.S., 2011. Multiangle implementation of atmospheric correction (MAIAC): 2. Aerosol algorithm. J. Geophys. Res. 116 (D3), D03211. https://doi.org/10.1029/2010JD014986.

Lyapustin, A., Wang, Y., Laszlo, I., Korkin, S., 2012. Improved cloud and snow screening in MAIAC aerosol retrievals using spectral and spatial analysis. Atmos. Meas. Tech. 5 (4), 843–850. https://doi.org/10.5194/amt-5-843-2012.

Lyapustin, A., Wang, Y., Korkin, S., Huang, D., 2018. MODIS collection 6 MAIAC algorithm. Atmos. Meas. Tech. 11 (10), 5741–5765. https://doi.org/10.5194/amt-11-5741-2018.

Mansoor, S., Farooq, I., Kachroo, M.M., Mahmoud, A.E.D., Fawzy, M., Popescu, S.M., Alyemeni, M.N., Sonne, C., Rinklebe, J., Ahmad, P., 2022. Elevation in wildfire frequencies with respect to the climate change. J. Environ. Manag. 301, 113769. https://doi.org/10.1016/J.JENVMAN.2021.113769.

Martin, S.T., Andreae, M.O., Artaxo, P., Baumgardner, D., Chen, Q., Goldstein, A.H., Guenther, A., Heald, C.L., Mayol-Bracero, O.L., McMurry, P.H., Pauliquevis, T., Pöschl, U., Prather, K.A., Roberts, G.C., Saleska, S.R., Silva Dias, M.A., Spracklen, D. V., Swietlicki, E., Trebs, I., 2010. Sources and properties of Amazonian aerosol particles. Rev. Geophys. 48 (2). https://doi.org/10.1029/2008RG000280.

Martins, V.S., Lyapustin, A., de Carvalho, L.A.S., Barbosa, C.C.F., Novo, E.M.L.M., 2017. Validation of high-resolution MAIAC aerosol product over South America. J. Geophys. Res. Atmos. 122 (14), 7537–7559. https://doi.org/10.1002/2016JD026301.

Mhawish, A., Banerjee, T., Sorek-Hamer, M., Lyapustin, A., Broday, D.M., Chatfield, R., 2019. Comparison and evaluation of MODIS Multi-angle implementation of atmospheric correction (MAIAC) aerosol product over South Asia. Rem. Sens. Environ. 224, 12–28. https://doi.org/10.1016/j.rse.2019.01.033.

Mielonen, T., Arola, A., Komppula, M., Kukkonen, J., Koskinen, J., de Leeuw, G., Lehtinen, K.E.J., 2009. Comparison of CALIOP level 2 aerosol subtypes to aerosol types derived from AERONET inversion data. Geophys. Res. Lett. 36 (18). https://doi.org/10.1029/2009GL039609.

Mollinedo, E.M., Krecl, P., Targino, A.C., Moreno, R.C.I., 2023. From lowland plains to the Altiplano: the impacts of regional transport of wildfire smoke on the air quality

of Bolivian cities. Atmos. Environ. 315, 120137. https://doi.org/10.1016/J.ATMOSENV.2023.120137.
Mulena, G.C., Asmi, E.M., Ruiz, J.J., Pallotta, J.V., Jin, Y., 2024. Biomass burning aerosol observations and transport over Northern and central Argentina: a case study. Remote Sens. 16 (10), 1780. https://doi.org/10.3390/rs16101780.
Osorio, M., Agesta, A., Bösch, T., Casaballe, N., Richter, A., Alvarado, L.M.A., Frins, E., 2024. Measurement report: combined use of MAX-DOAS and AERONET ground-based measurements in Montevideo, Uruguay, for the detection of distant biomass burning. Atmos. Chem. Phys. 24 (12), 7447–7465. https://doi.org/10.5194/acp-24-7447-2024.
Otero, L.A., Ristori, P.R., Pallotta, J.V., Pawelko, E.E., Ballesteros, P.A., Orte, P.F., Nicora, G., Raponi, M.M., D'Elía, R., Wolfram, E., Salvador, J., Bulnes, D., Martorella, E., Pereyra, A., González, F., Vilar, O., Dworniczak, J.C., Quel, E.J., 2013. Eruption of Puyehue - cordón caulle: early warning of the phenomenon and measurement of the ashes in Buenos Aires, Argentina, June 2011. Anales AFA 23 (1), 148–152. https://doi.org/10.31527/analesafa.2013.23.1.148.
Otero, L., Casasola, F., Pereyra, C., Prieto, M., Brusca, S., Ristori, P., 2020. Australian aerosol layers over Argentine territory during November 2019. Anales AFA 31 (1), 1–6. https://doi.org/10.31527/analesafa.2020.31.1.1.
Peel, M.C., Finlayson, B.L., McMahon, T.A., 2007. Updated world map of the Köppen-Geiger climate classification. Hydrol. Earth Syst. Sci. 11 (5), 1633–1644. https://doi.org/10.5194/hess-11-1633-2007.
Qin, W., Fang, H., Wang, L., Wei, J., Zhang, M., Su, X., Bilal, M., Liang, X., 2021. MODIS high-resolution MAIAC aerosol product: global validation and analysis. Atmos. Environ. 264, 118684. https://doi.org/10.1016/j.atmosenv.2021.118684.
Reis, M., Graça, P.M.L.D.A., Yanai, A.M., Ramos, C.J.P., Fearnside, P.M., 2021. Forest fires and deforestation in the central Amazon: effects of landscape and climate on spatial and temporal dynamics. J. Environ. Manag. 288, 112310. https://doi.org/10.1016/J.JENVMAN.2021.112310.
Remer, L.A., Levy, R.C., Martins, J.V., 2024. Opinion: aerosol remote sensing over the next 20 years. Atmos. Chem. Phys. 24 (4), 2113–2127. https://doi.org/10.5194/acp-24-2113-2024.
Rizzo, L.V., Correia, A.L., Artaxo, P., Procópio, A.S., Andreae, M.O., 2011. Spectral dependence of aerosol light absorption over the Amazon Basin. Atmos. Chem. Phys. 11 (17), 8899–8912. https://doi.org/10.5194/acp-11-8899-2011.
Roberts, G., Wooster, M.J., 2021. Global impact of landscape fire emissions on surface level $PM_{2.5}$ concentrations, air quality exposure and population mortality. Atmos. Environ. 252, 118210. https://doi.org/10.1016/j.atmosenv.2021.118210.
Rongbin, X., Pei, Y., J, A.M., H, J.F., M, S.J., L, B.M., Andy, H., L, E.K., Shanshan, L., Yuming, G., 2020. Wildfires, global climate change, and human health. N. Engl. J. Med. 383 (22), 2173–2181. https://doi.org/10.1056/NEJMsr2028985.
San Martín, R., Ottlé, C., Sörensson, A., 2023. Fires in the South American Chaco, from dry forests to wetlands: response to climate depends on land cover. Fire Ecol. 19 (1), 57. https://doi.org/10.1186/s42408-023-00212-4.
Sayer, A.M., Hsu, N.C., Bettenhausen, C., Jeong, M.-J., 2013. Validation and uncertainty estimate for MODIS Collection 6 "Deep Blue" aerosol data. J. Geophys. Res. Atmos. 118 (14), 7864–7872. https://doi.org/10.1002/jgrd.50600.
Schroeder, W., Oliva, P., Giglio, L., Csiszar, I.A., 2014. The New VIIRS 375 m active fire detection data product: algorithm description and initial assessment. Rem. Sens. Environ. 143, 85–96. https://doi.org/10.1016/j.rse.2013.12.008.
Si, Y., Lu, Q., Zhang, X., Hu, X., Wang, F., Li, L., Gu, S., 2021. A review of advances in the retrieval of aerosol properties by remote sensing multi-angle technology. Atmos. Environ. 244, 117928. https://doi.org/10.1016/J.ATMOSENV.2020.117928.
Silvestrini, R.A., Soares-Filho, B.S., Nepstad, D., Coe, M., Rodrigues, H., Assunção, R., 2011. Simulating fire regimes in the Amazon in response to climate change and deforestation. Ecol. Appl. 21 (5), 1573–1590. https://doi.org/10.1890/10-0827.1.
Smichowski, H., Contreras, F.I., 2024. Application of Google Earth Engine in the preliminary analysis of fire severity in the Iberá National Park and Reserve, Argentina. Revista UDCA Actualidad & Divulgación Científica 27 (1). https://doi.org/10.31910/rudca.v27.n1.2024.2464.
Souto-Oliveira, C.E., Marques, M.T.A., Nogueira, T., Lopes, F.J.S., Medeiros, J.A.G., Medeiros, I.M.M.A., Moreira, G.A., da Silva Dias, P.L., Landulfo, E., Andrade, M. de F., 2023. Impact of extreme wildfires from the Brazilian forests and sugarcane burning on the air quality of the biggest megacity on South America. Sci. Total Environ. 888, 163439. https://doi.org/10.1016/j.scitotenv.2023.163439.
Ştefănie, H.I., Radovici, A., Mereuță, A., Arghiuș, V., Cămărășan, H., Costin, D., Botezan, C., Gînscă, C., Ajtai, N., 2023. Variation of aerosol optical properties over Cluj-Napoca, Romania, based on 10 years of AERONET data and MODIS MAIAC AOD product. Remote Sens. 15 (12), 3072. https://doi.org/10.3390/rs15123072.
Superczynski, S.D., Kondragunta, S., Lyapustin, A.I., 2017. Evaluation of the multi-angle implementation of atmospheric correction (MAIAC) aerosol algorithm through intercomparison with VIIRS aerosol products and AERONET. J. Geophys. Res. Atmos. 122 (5), 3005–3022. https://doi.org/10.1002/2016JD025720.
Takemura, T., Nakajima, T., Dubovik, O., Holben, B.N., Kinne, S., 2002. Single-Scattering albedo and radiative forcing of various aerosol species with a global three-dimensional model. J. Clim. 15 (4), 333–352. https://doi.org/10.1175/1520-0442(2002)015<0333:SSAARF>2.0.CO;2.
Tuccella, P., di Antonio, L., di Muzio, A., Colaiuda, V., Lidori, R., Menut, L., Pitari, G., Raparelli, E., 2025. Modeling the black and brown carbon absorption and their radiative impact: the June 2023 intense Canadian boreal wildfires case study. J. Geophys. Res. Atmos. 130 (7). https://doi.org/10.1029/2024JD042674.
Ulke, G.A., Maria, K., de Freitas, S.R., 2011. Biomass burning in South America: transport patterns and impacts. In: Biomass - Detection, Production and Usage. InTech. https://doi.org/10.5772/19264.
Valle Seijo, M.F., 2025. AOD Analysis Using MAIAC and AERONET During the 2020 Wildfire Season in Southeastern South America (V1.0.0). Zenodo. https://doi.org/10.5281/zenodo.14740511.
Valle Seijo, M.F., Micheletti, M.I., Otero, L.A., Piacentini, R.D., 2024a. Atmospheric pollutants in Rosario, Argentina analysed through remote sensing: wildfires and COVID-19 lockdown effects. Remote Sens. Appl.: Soc. Environ. 36, 101326. https://doi.org/10.1016/j.rsase.2024.101326.
Valle Seijo, M.F., Otero, L.A., Piacentini, R.D., 2024b. Spatio-temporal analysis of fire events over the past 10 years in the central-east region of Argentina and surrounding areas. In: 2024 IEEE Biennial Congress of Argentina (ARGENCON), pp. 1–8. https://doi.org/10.1109/ARGENCON62399.2024.10735824.
Vieira, E.V.R., Rosario, N.E.D., Yamasoe, M.A., Morais, F.G., Martinez, P.J.P., Landulfo, E., De Miranda, R.M., 2023. Chemical characterization and optical properties of the aerosol in São Paulo, Brazil. Atmosphere 14 (9), 1460. https://doi.org/10.3390/atmos14091460.
World Health Organization, 2021. WHO Global Air Quality Guidelines: Particulate Matter ($PM_{2.5}$ and PM_{10}), Ozone, Nitrogen Dioxide, Sulfur Dioxide and Carbon Monoxide.
Zhang, Z., Wu, W., Fan, M., Wei, J., Tan, Y., Wang, Q., 2019. Evaluation of MAIAC aerosol retrievals over China. Atmos. Environ. 202, 8–16. https://doi.org/10.1016/j.atmosenv.2019.01.013.